Supporting Information

Förster Resonance Energy Transfer Drives Higher Efficiency in Ternary Blend Organic Solar Cells

Aiswarya Abhisek Mohapatra,[a] Vincent Kim,[b] Boregowda Puttaraju,[a] Aditya Sadhanala,[b] Xuechen Jiao,[c,d] Christopher R. McNeill,[c] Richard H. Friend,[b] Satish Patil [a*]

[a]Solid State and Structural Chemistry Unit, Indian Institute of Science, Bangalore, India 560012

[b]Cavendish Laboratory, Department of Physics, University of Cambridge, Cambridge, CB3 0HE, UK

[c]Department of Materials Science and Engineering, Monash University, Clayton, VIC, 3800, Australia

[d]Australian Synchrotron, ANSTO, Clayton, Victoria, 3168, Australia

Corresponding author's E-mail: spatil@iisc.ac.in

Table of Contents for Supporting Information

Materials and Methods

Analytical grade acetone, isopropanol, chloroform, 1,2-dichlorobenzene and 1-chloronaphthalene, zinc acetate dihydrate, ethanolamine and 2-methoxyethanol for device fabrication were purchased from Sigma-Aldrich. P3HT was purchased from Rieke Metals. $PC_{71}BM$ was purchased from Solenne B.V. Pre-patterned ITO coated glass substrates (12 × 12 × 1.1 mm with 7 mm ITO stripe) were purchased from Colorado Concept Coatings, U.S. The required monomers [4,8-bis(5-(2-ethylhexyl)thiophen-2-yl)benzo[1,2-b:4,5-b']dithiophene-2,6-diyl] bis(trimethylstannane) **(M1)** and 3-(5-bromothiophen-2-yl)-2,5-bis(2-octyldodecyl)-6-(5-phenylthiophen-2-yl)pyrrolo[3,4-c]pyrrole-1,4(2H,5H)-dione **(M2)** were synthesized using the procedure reported in literature.[1] All the reagents and solvents for synthesis were purchased from Sigma-Aldrich and used without further purification.

The ^{1}H and ^{13}C NMR spectra of 2DPP-BDT were recorded using Bruker Avance 400 MHz and 100 MHz frequency NMR spectrometer, respectively. $CDCl_3$ and TMS were used as solvent and internal standard, respectively. Matrix-assisted laser desorption/ionization-time of flight mass spectroscopy (MALDI-TOF MS) was performed in Bruker Microflex instrument. Thin films of 2DPP-BDT, all the binary and ternary blends were prepared by spinning their dissolved solutions in respective solvents at 1000 rpm on pre-cleaned ozone-treated quartz substrates and UV-Visible absorption spectra were recorded using PerkinElmer (Lambda 35) spectrometer in ambient conditions. The fluorescence spectra for the neat P3HT, neat 2DPP-BDT films and films with varying ratio of second components for photoluminescence quenching studies were collected using Horiba Jobin Yvon Fluorolog4 fluorometer. The P3HT:2DPP-BDT films were excited at 554 nm and the 2DPP-BDT:$PC_{71}BM$ films were excited at 710 nm and the corresponding emission spectra were recorded in ambient conditions. Atomic Force Microscopy (AFM) images for all the blends were recorded by using Bruker AFM instrument in tapping mode. Thin films of binary blends and the ternary blend with additive were prepared by dissolving them in chloroform followed by spin-coating onto pre-cleaned ozone-treated Si wafers. Samples for photoemission spectroscopy (PES) were fabricated on Au/Cr/Si substrates. Oligomer samples were deposited directly onto the substrates by spin-casting to give films of approximately 100 nm thicknesses. All the PES samples were measured inside ultrahigh vacuum (UHV) chamber (ESCALAB 250Xi) for ultraviolet photoelectron spectroscopy (UPS) measurements. UPS measurements were performed using a double-differentially pumped He gas discharge lamp emitting He I radiation (hv = 21.22 eV) with a pass energy of 5 eV/h. The bright field transmission electron microscopy (TEM) imaging was

performed using a JEOL 2100F TEM equipped with a field emission gun (FEG). The operating voltage of the FEG was 80 kV.

Both binary and ternary blend solar cells were fabricated in inverted device geometry (ITO/ZnO/active layer/MoO_3/Ag). For P3HT:$PC_{71}BM$ blend solar cells, 18 mg/mL P3HT and 12 mg/mL $PC_{71}BM$ were dissolved in 1,2-dichlorobenzene. 7 mg/mL of both 2DPP-BDT and $PC_{71}BM$ were dissolved in $CHCl_3$ for 2DPP-BDT:$PC_{71}BM$ blend solar cells. For ternary blend, the weight ratio of each component was 20 mg/mL in $CHCl_3$. 0.8:0.2:1 was the optimal weight ratio of P3HT:2DPP-BDT:$PC_{71}BM$ for which maximum device performance was achieved after addition of 1 volume% 1-chloronaphthalene. For device fabrication, pre-patterned ITO substrates were cleaned by ultrasonic treatment in soap solution, de-ionized water, acetone and isopropanol, sequentially, for 10 min each. Then the substrates were dried with N_2 flow, followed by oxygen-plasma treatment for 10 min. A thin layer (≈30 nm) of ZnO was prepared by spin-coating (at 5000 rpm for 60 s) from a precursor solution of zinc acetate dihydrate (1.00 g) and ethanolamine (0.28 g) in 2-methoxyethanol (10 mL), followed by baking at 200 °C for 10 min under air.[1] The photoactive layers were then deposited by spin coating at 1000 rpm for 60 sec from respective solutions of binary or ternary blends. The films of P3HT:$PC_{71}BM$ and ternary blend were then annealed at 140 °C for 15 min under N_2 atmosphere. Finally, MoO_3 (10 nm) and then Ag (100 nm) were deposited on top of the active layer using a shadow mask, defining the pixel area of 4.5 mm^2, in a thermal evaporator at a pressure less than $4x10^{-6}$ Torr.

The photocurrent density-voltage (*J-V*) characteristics of all the devices were measured in air using a KHS 575 solar simulator with an AM 1.5G spectrum calibrated to 1 sun using a pyranometer. Light-intensity-dependent measurements were carried out under the same solar simulator using a combination of a series of attenuators (23% –100%) that changes the light level of the solar simulator. External quantum efficiency (EQE) measurements were performed to measure the photoresponse as a function of photon energy using light from an Oriel Cornerstone 260 monochromator. EQEs were calculated from this, comparing the solar cell photoresponse to the response from a reference diode. For transient absorption spectroscopy measurements, a 1kHz regenerative Ti:sapphire amplifier (Solstice Ace, Spectra-Physics) with an 800nm output was used and part of the Solstice Ace output was sent into a home-built non-collinear optical parametric amplifier (NOPA) which acted as a broadband visible probe and was split into a probe and reference. Another part of the Solstice output was sent through another home-built NOPA which delivered a tuneable excitation pulse. A chopper wheel was set to rotate at 500Hz, which blocks the pump while a computer-operated mechanical delay

stage (Newport) controls the delay between the pump and the probe. We sent the probe and reference through an imaging spectrometer (Shamrock SR 303i, Andor Technology) and a pair of linear image sensors (G11608, Hamamatsu) detected them. A custom-built board from Stresing Entwicklungsburo runs and reads the image sensors at 1 kHz. Grazing-incidence wide-angle X-ray scattering (GIWAXS) measurements were collected at the small and wide angle X-ray scattering beamline at the Australian Synchrotron.[2] The detector utilized was a Pilatus 1M active pixel 2D detector with 0.172 mm × 0.172 mm pixels, in integration mode, positioned approximately 400 mm from the sample location. The precise sample-to-detector distance was determined with a silver behenate standard. 15 KeV incident X-ray focused to approximately a 0.25 mm × 0.1 mm spot was used to provide large enough q space. An angle of incidence close to the critical angle was used, chosen as the angle that maximised the scattering intensity. The 2D raw data was reduced and analysed with a modified version of Nika.[3]

Synthesis of 2DPP-BDT

Scheme S1. Synthetic scheme for 2DPP-BDT

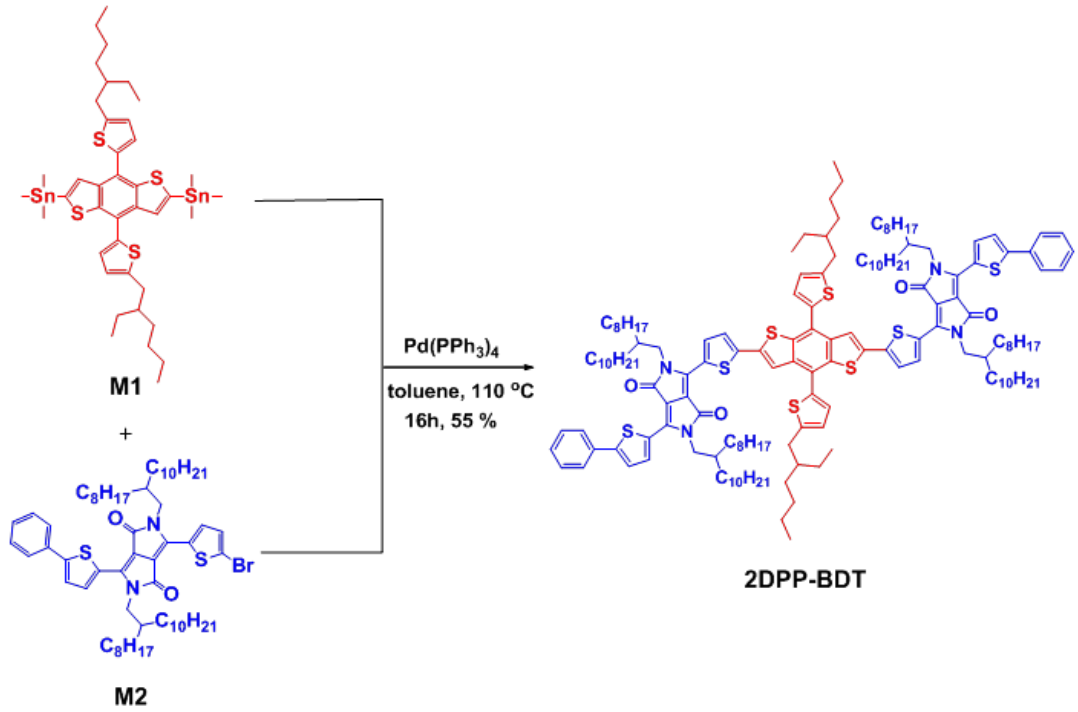

To a schlenk tube was added [4,8-bis(5-(2-ethylhexyl)thiophen-2-yl)benzo[1,2-b:4,5-b']dithiophene-2,6-diyl]bis(trimethylstannane) **(M1)** (0.1g, 0.11mmol) and 3-(5-bromothiophen-2-yl)-2,5-bis(2-octyldodecyl)-6-(5-phenylthiophen-2-yl)pyrrolo [3,4-c]Pyrrole-1,4(2H,5H)-dione **(M2)** (0.22g, 0.22mmol). Toluene (20 mL) was added, the

reaction mixture was degassed before addition of catalyst $Pd(PPh_3)_4$ (10 mg), Then the reaction mixture was refluxed at 110 °C for 24 h. The resulting mixture was cooled to room temperature and quenched with 1M HCl (10 mL) and washed with EDTA solution, extracted with chloroform and dried over anhydrous Na_2SO_4, the organic layer was evaporated, and the crude product was purified by preparative chromatography (ethyl acetate/hexane 1:9) to afford dark blue solid (0.15g, 55%).

^{1}H NMR (400 MHz, $CDCl_3$) δ 8.97 (d, *J* = 4Hz, 3H), 8.93 (d, *J* = 4Hz, 2H), 7.71 (br, s, 2H), 7.62 (d, *J* = 8Hz, 4H), 7.41 (d, *J* = 4Hz, 2H), 7.37 (d, *J* = 4Hz, 5H), 7.34-7.31 (m, 5H), 6.98 (d, *J* = 4Hz, 2H), 4.01 (br, s, 8H), 2.95 (d, *J* = 4Hz 4H), 1.95 (br, s, 4H), 1.80-1.77 (m, 2H), 1.45-1.39 (m, 10H), 1.33-1.32 (m, 20H), 1.21-1.18 (m, 100H), 1.04 (t, *J* = 8Hz, 8H), 0.98 (t, *J* = 4Hz, 8H), 0.85-0.79 (m, 30H) ppm. ^{13}C NMR (100 MHz, $CDCl_3$) δ 161.56, 146.35, 145.50, 142.08, 138.95, 137.52, 137.04, 136.49, 133.42, 133.13, 132.96, 129.10, 128.77, 128.07, 125.99, 125.59, 124.37, 121.10, 108.25, 46.33, 41.51, 38.01, 34.48, 31.94, 31.92, 31.42, 31.20, 30.69, 30.10, 29.68, 29.62, 29.57, 29.38, 29.34, 29.00, 26.47, 26.26, 25.83, 23.10, 22.69, 14.23, 14.11, 14.09, 10.98 ppm. MALDI-TOF MS (*m/z*): calculated for $C_{154}H_{222}N_4O_4S_8$: 2448.50; found, 2449.25 (M+1)

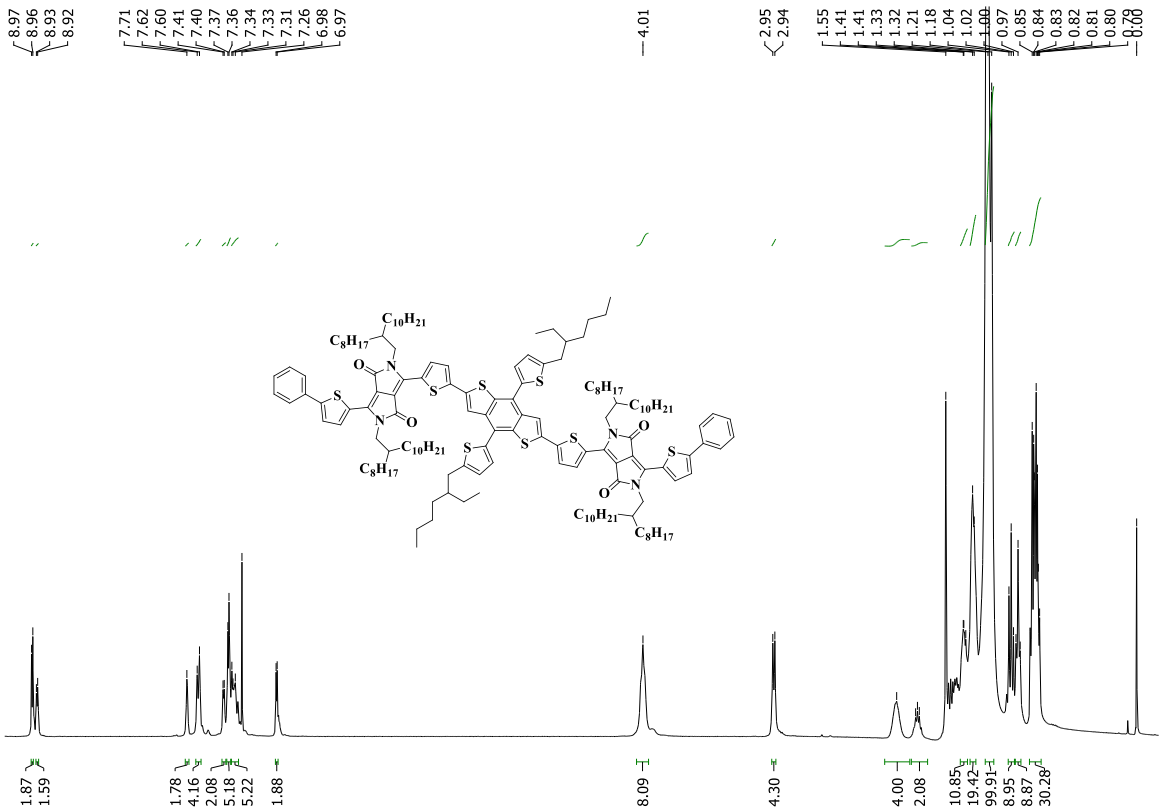

Figure S1. ^{1}H NMR of 2DPP-BDT

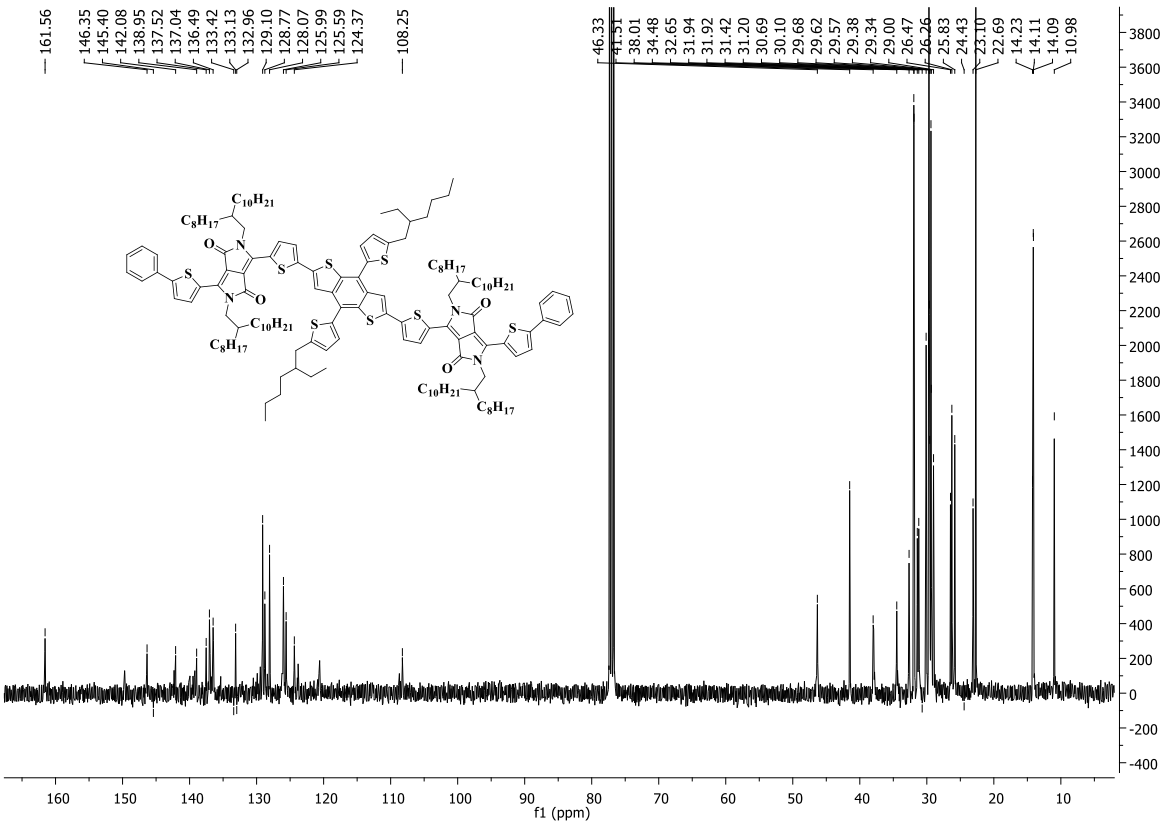

Figure S2. ^{13}C NMR of 2DPP-BDT

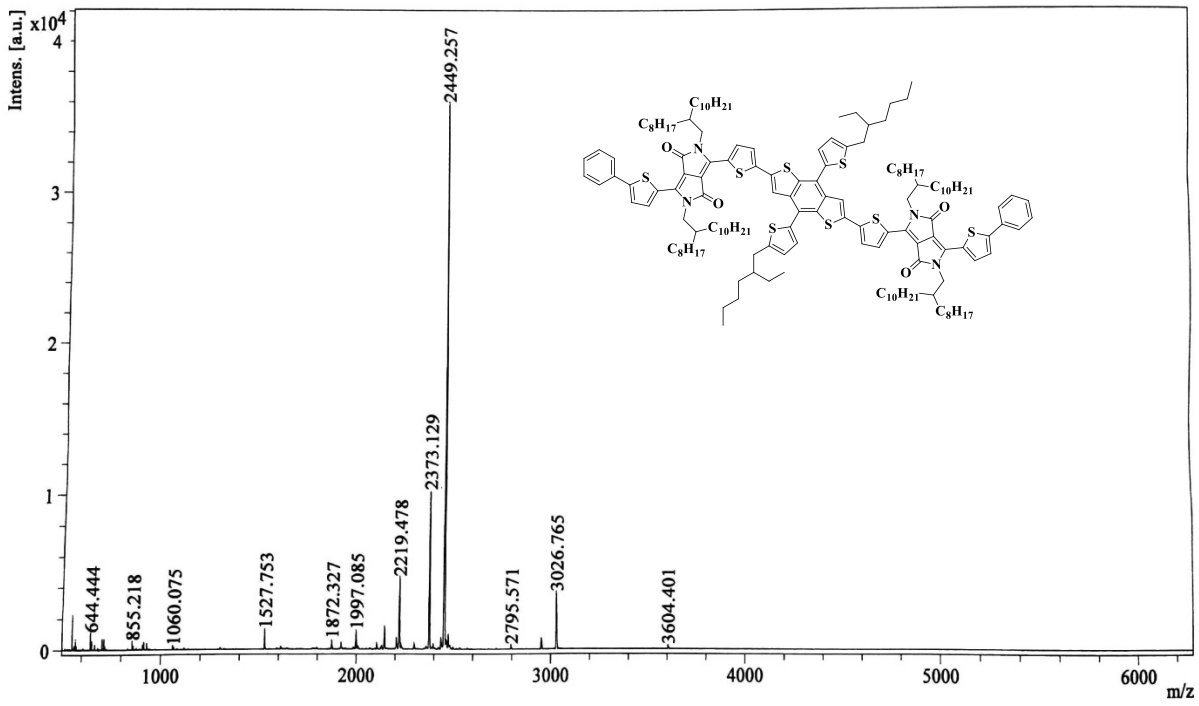

Figure S3. MALDI-TOF MS of 2DPP-BDT

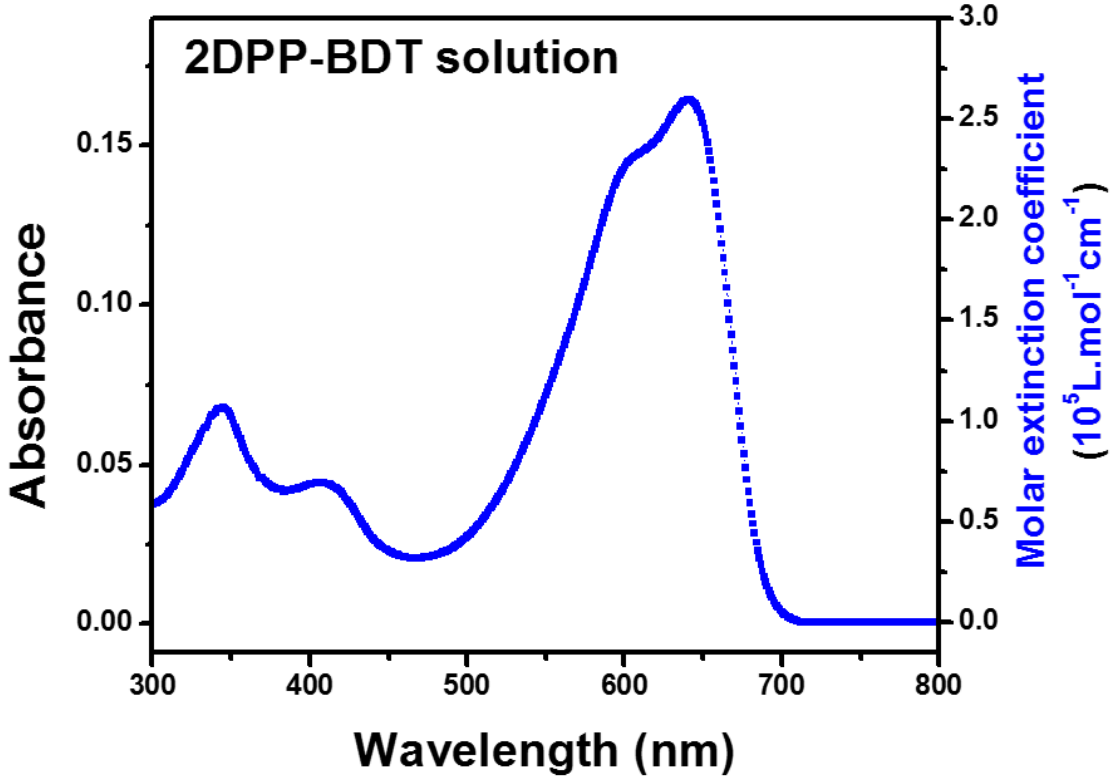

Figure S4. Solution phase UV-vis absorption spectrum of 2DPP-BDT showing high molar extinction coefficient (2.54 x 10^5 $L.mol^{-1}.cm^{-1}$) at absorption maximum

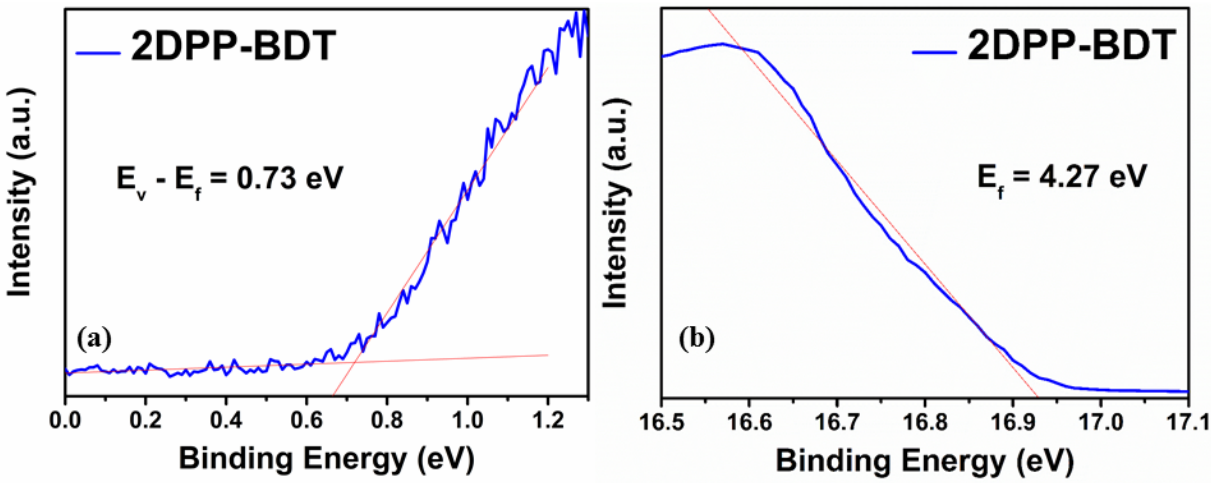

Figure S5. Ultraviolet photoelectronic spectroscopy (UPS) **(a)** extraction of Fermi levels and **(b)** valence Band Energies

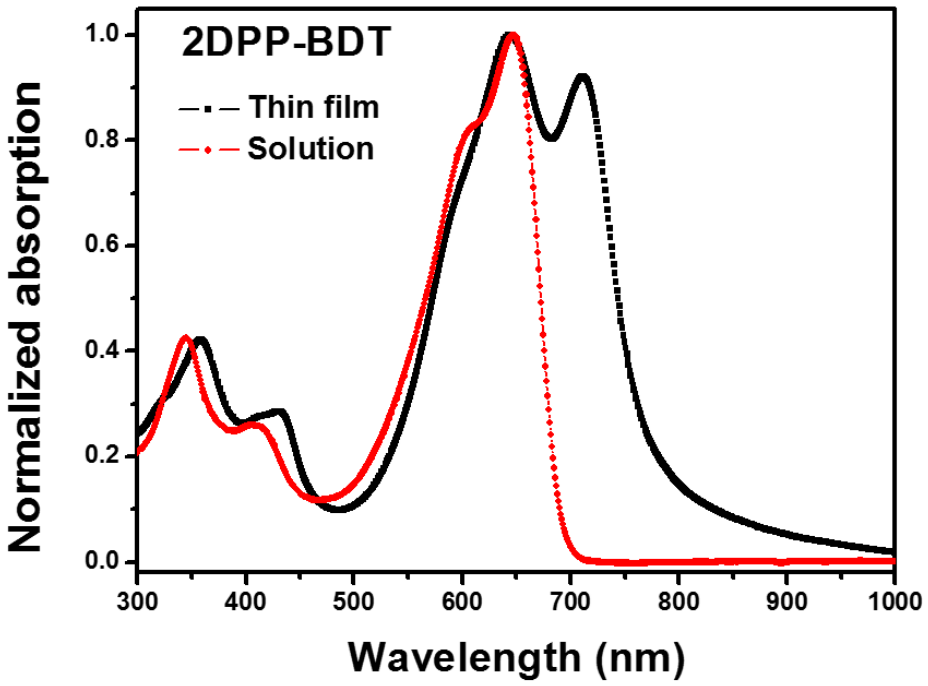

Figure S6. The UV-Vis absorption spectra of 2DPP-BDT both in solid state and solution phase

Förster distance, $\mathbf{R_0}$, at which the energy-transfer efficiency is 50% is estimated using the following equation [4]

$$R_0 = (0.211)\,(\varkappa^2 n^{-4} Q_D J(\lambda))^{1/6} \qquad \text{(in Å)}$$

Where, $J(\lambda) = \int F_D(\lambda)\,\varepsilon_A(\lambda)\,\lambda^4\,d\lambda \,/\, \int F_D(\lambda) d\lambda$

$\varkappa$ is the orientation factor between the donor and acceptor dipoles;

$\mathbf{Q_D}$ is the average donor fluorescence quantum yield in the absence of the acceptor;

n is the medium refractive index;

J (λ) represents the overlap integral, characterized by normalized spectrum overlap between donor molecule's $F_D(\lambda)$, fluorescence intensity in arbitrary unit and $\varepsilon_A(\lambda)$, acceptor's absorption coefficient in cm^{-1} scaled by λ, wavelength (in nm) to the fourth power.

$\kappa^2 = 2/3$ for random orientation of dipoles; **n** = 1.5 (for most organic systems);

$Q_D = 0.1$ (for P3HT, in chloroform); **J(λ) =** $4.99 * 10^{14}\ cm^{-1}\ nm^4$

Substituting the above values in the equation, we found the Förster distance, R_0 to be **18.19 Å**

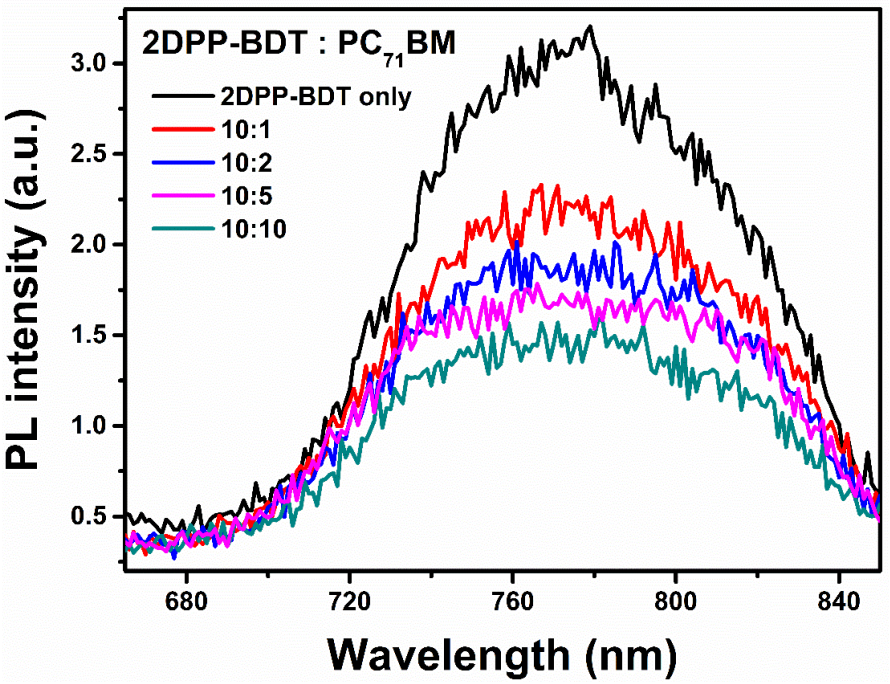

Figure S7. Photoluminescence quenching of 2DPP-BDT upon addition of $PC_{71}BM$

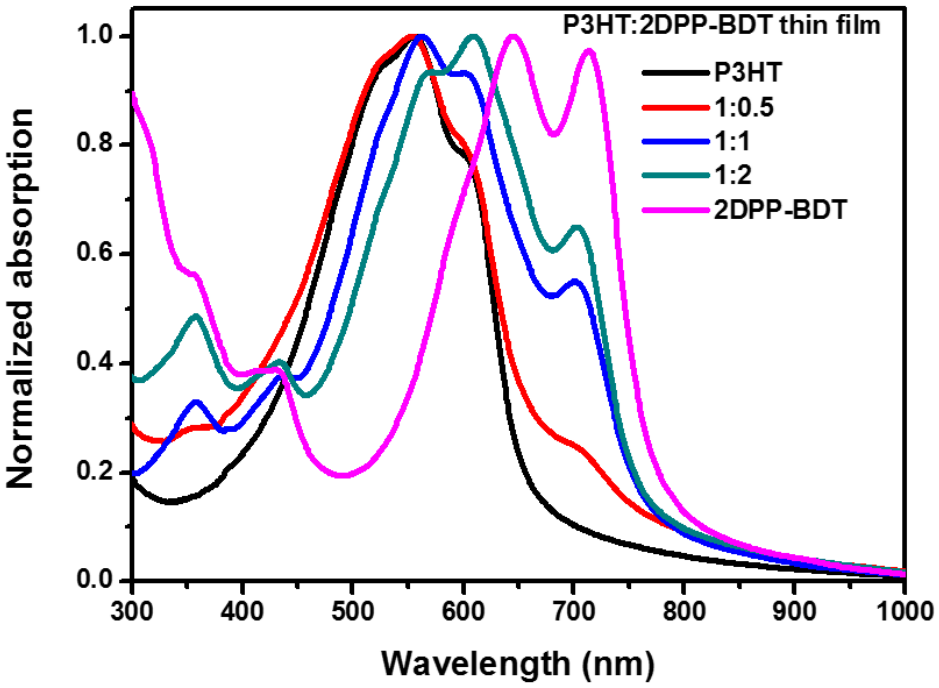

Figure S8. Normalized thin film UV-Vis absorption spectra of P3HT, 2DPP-BDT and P3HT:2DPP-BDT blends

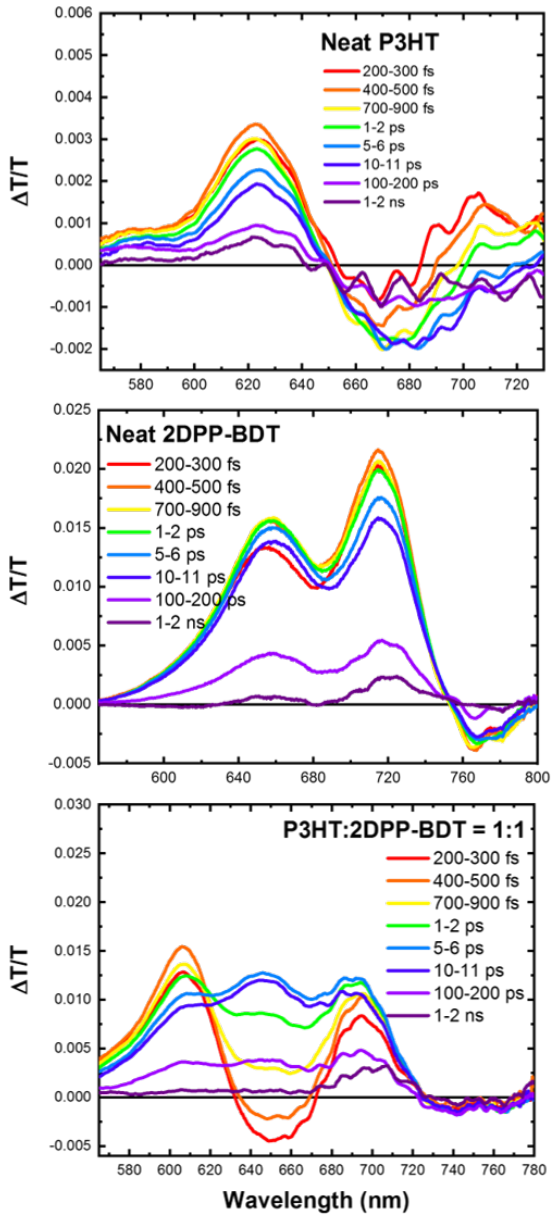

Figure S9. Transient absorption spectra of the neat components and P3HT:2DPP-BDT (1:1) blend films

Table S1. Thickness dependent performances of ternary blend solar cells*

Average thickness of ternary blend active layer (nm)	V_{oc} (V)	J_{sc} (mA.cm^{-2})	Fill factor (%)	PCE (%)	
				Average	Best
179[a]	0.56 ± 0.08	5.52 ± 0.45	34.68 ± 5.17	1.06 ± 0.08	1.16
202[b]	0.59 ± 0.04	5.98 ± 0.49	39.11 ± 5.10	1.41 ± 0.38	1.97
307	0.59 ± 0.02	11.85 ± 0.70	54.54 ± 2.30	3.80 ± 0.20	4.11

[a]statistics based on 5 individual devices; [b]statistics based on 10 individual devices
***the ternary blend solar cell has a weight ratio of P3HT:2DPP-BDT:$PC_{71}BM$ = 0.8:0.2:1 and processed with 1 volume % 1-CN in chloroform**

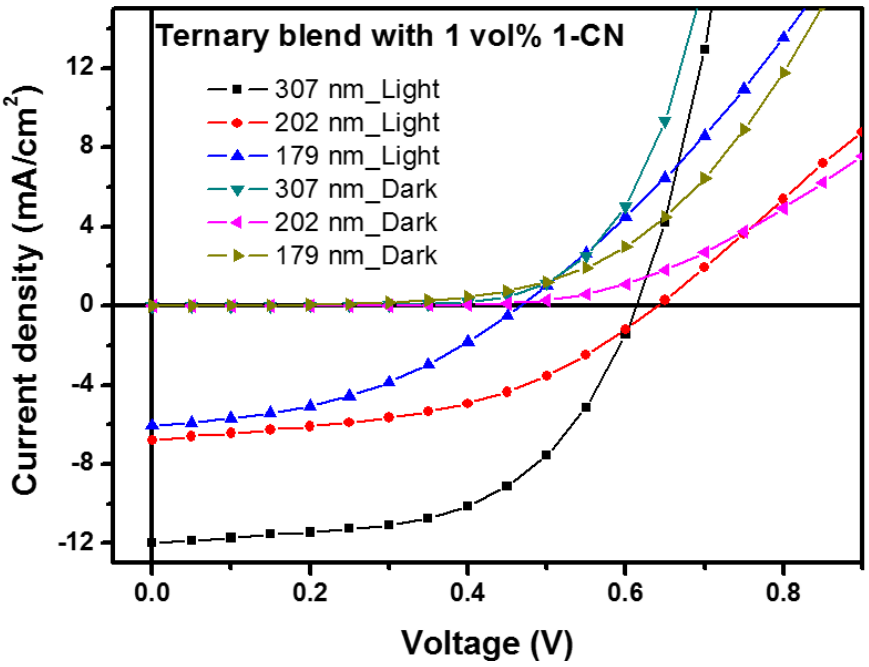

Figure S10. Compared J-V characteristics of the best performing ternary blend solar cells with different active layer thicknesses.

Table S2. Open circuit voltage of the ternary blends by varying the ratio of P3HT to 2DPP-BDT by weight.

Weight ratio P3HT : 2DPP-BDT : $PC_{71}BM$ (with 1 vol % 1-CN)	**V_{oc} (V)**
0.7 : 0.3 : 1	0.618 ± 0.006
0.8 : 0.2 : 1	0.610 ± 0.009
0.9 : 0.1 : 1	0.610 ± 0.006

Table S3. Series (R_s) and shunt (R_{sh}) resistances of the optimized binary and ternary blend solar cells.

Blends	**FF (%)**	**R_S (Ohm.cm²)**	**R_{Sh} (Ohm.cm²)**
P3HT:$PC_{71}BM$ (1.5:1)	65.0	482.8	820.3
P3HT:2DPP-BDT:$PC_{71}BM$ (0.8:0.2:1)(1 vol% 1-CN)	56.7	575.4	853.9

For an ideal solar cell, the R_s needs to be minimum and R_{sh} needs to be maximum. In the table above, the series resistance of the P3HT:$PC_{71}BM$ cell is less compared to the ternary blend which explains more squareness of the J-V curve of the P3HT:$PC_{71}BM$ cell. The series resistance gets affected by the carrier mobilities and contact resistances of the cell. We attribute the low R_s to better carrier mobilities in P3HT:$PC_{71}BM$ cell compared to the ternary blend and hence the better fill factor.

Table S4. The device parameters for ternary blend with and without additive treatment.

P3HT:2DPP-BDT:$PC_{71}BM$ 0.8:0.2:1	V_{oc} (V)		J_{sc} ($mA.cm^{-2}$)		FF (%)		PCE (%)	
	Average	Best	Average	Best	Average	Best	Average	Best
w/o additive*	0.64 ± 0.01	0.65	9.12 ± 0.43	9.37	41.32 ± 3.54	44.37	2.41 ± 0.30	2.69
1 vol% 1-CN*	0.59 ± 0.02	0.61	11.9 ± 0.70	11.88	54.5 ± 2.3	56.7	3.80 ± 0.20	4.11
The statistics in this table are based on 8*/10* individual devices								

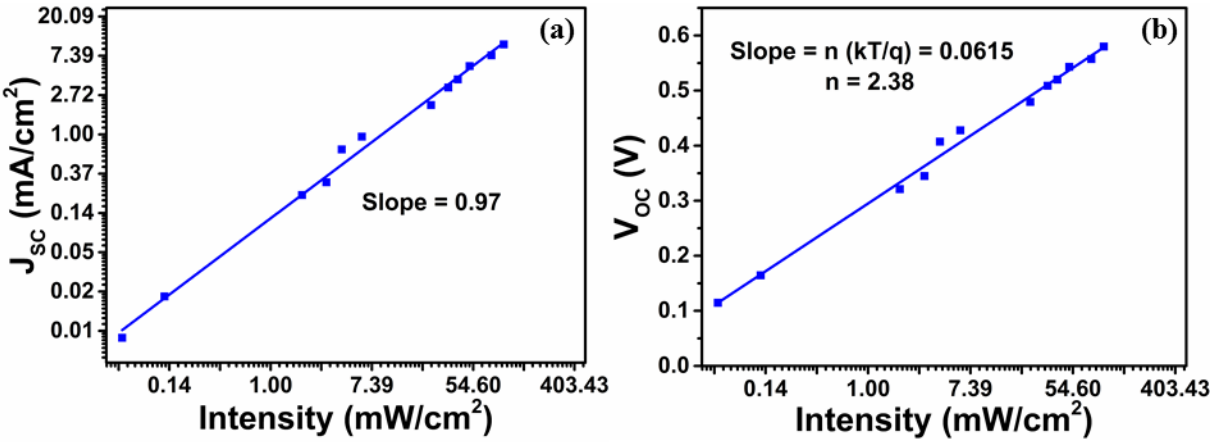

Figure S11. (a) Intensity vs. short-circuit current density plot of an optimized ternary blend device; **(b)** plot of intensity vs. open circuit voltage of the same.

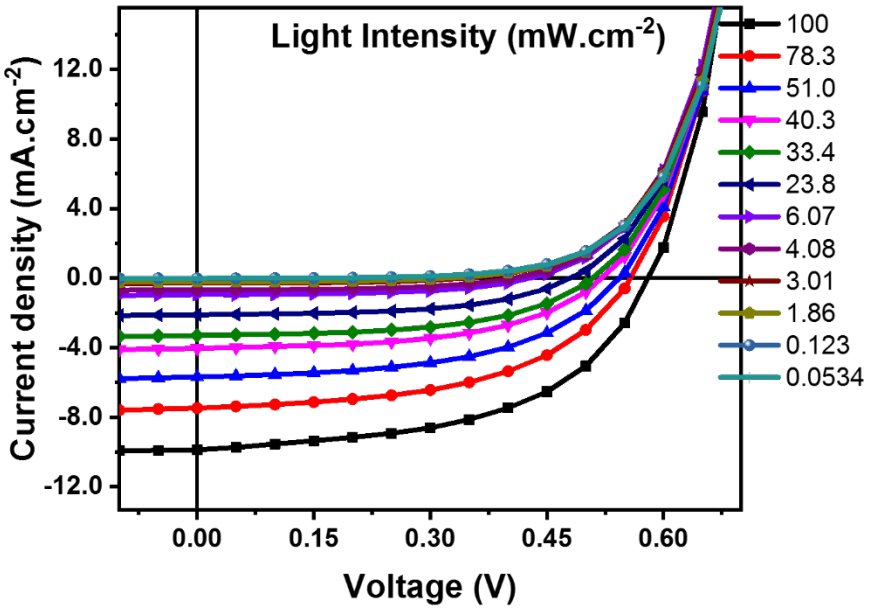

Figure S12. The intensity dependence of J-V characteristics of the ternary blend solar cell

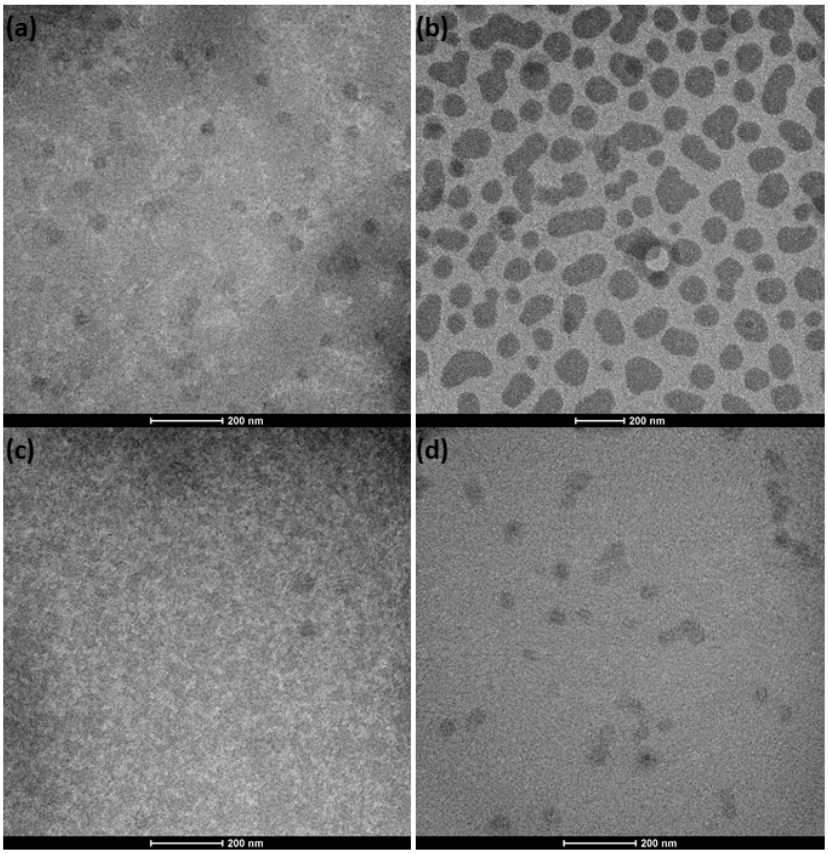

Figure S13. Bright-field TEM images of **(a)** P3HT:PC$_{71}$BM; **(b)** 2DPP-BDT:PC$_{71}$BM; ternary blend **(c)** without 1 vol% 1-CN **(d)** with 1 vol% 1-CN

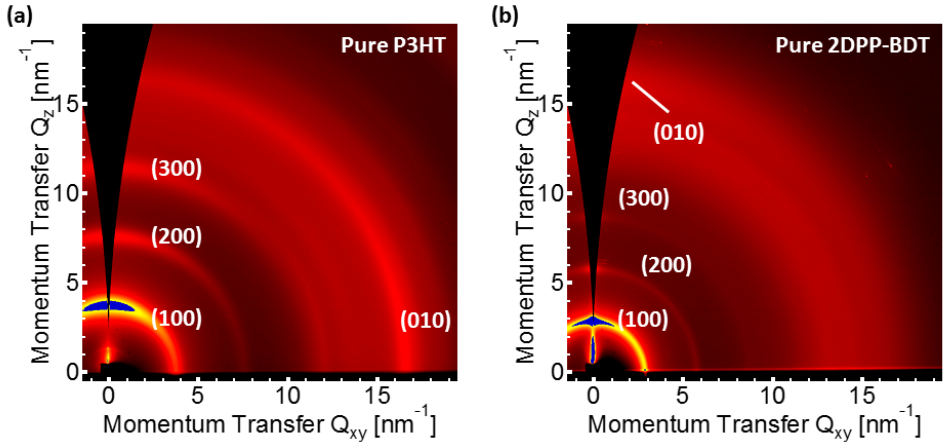

Figure S14. 2D GIWAXS for pure P3HT **(a)** and 2DPP-BDT **(b)**. The simultaneous appearance of out-of-plane (h00) and in-plane (010) from P3HT thin film indicates the preferential edge-on orientation adopted by the P3HT crystallites, while the co-existence of out-of-plane (h00) and (010) from 2DPP-BDT suggests that 2DPP-BDT crystallites adopt rolling-log arrangement within the thin film.

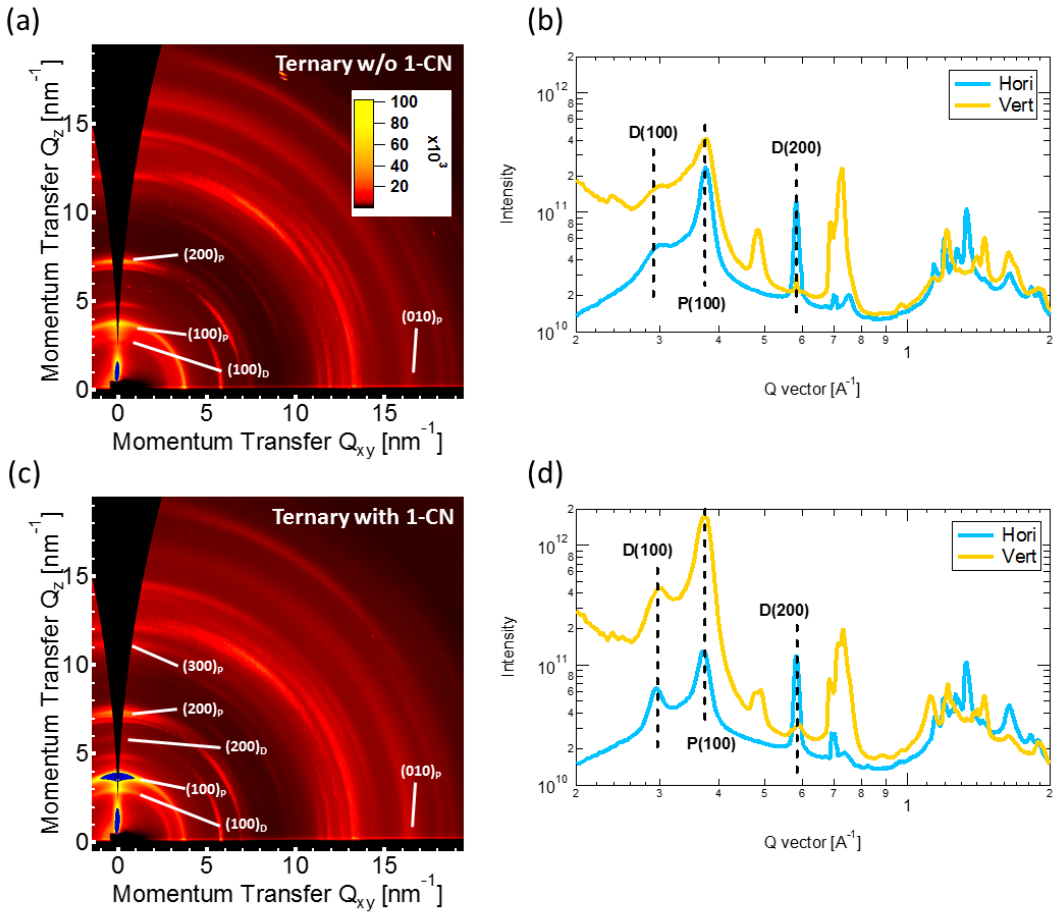

Figure S15. 2D GIWAXS patterns of the thermally annealed P3HT:2DPP-BDT:PC$_{71}$BM ternary blends processed without **(a)** and with 1-chloronaphthalene (1-CN) additive **(c)** and the associated 1D GIWAXS profiles along OOP (vertical to the substrate) and IP (horizontal to the substrate) **(b)** & **(d)**. The subscript D denotes 2DPP-BDT and P denotes P3HT. Note that both 2D patterns and 1D profiles are plotted using the identical intensity scales. Thereby a direct comparison between samples with comparable thickness is feasible. It can be clearly seen that the use of 1-CN additive enhances the overall diffraction intensity and the 2DPP-BDT lamellar diffraction intensity relative to P3HT lamellar diffraction intensity.

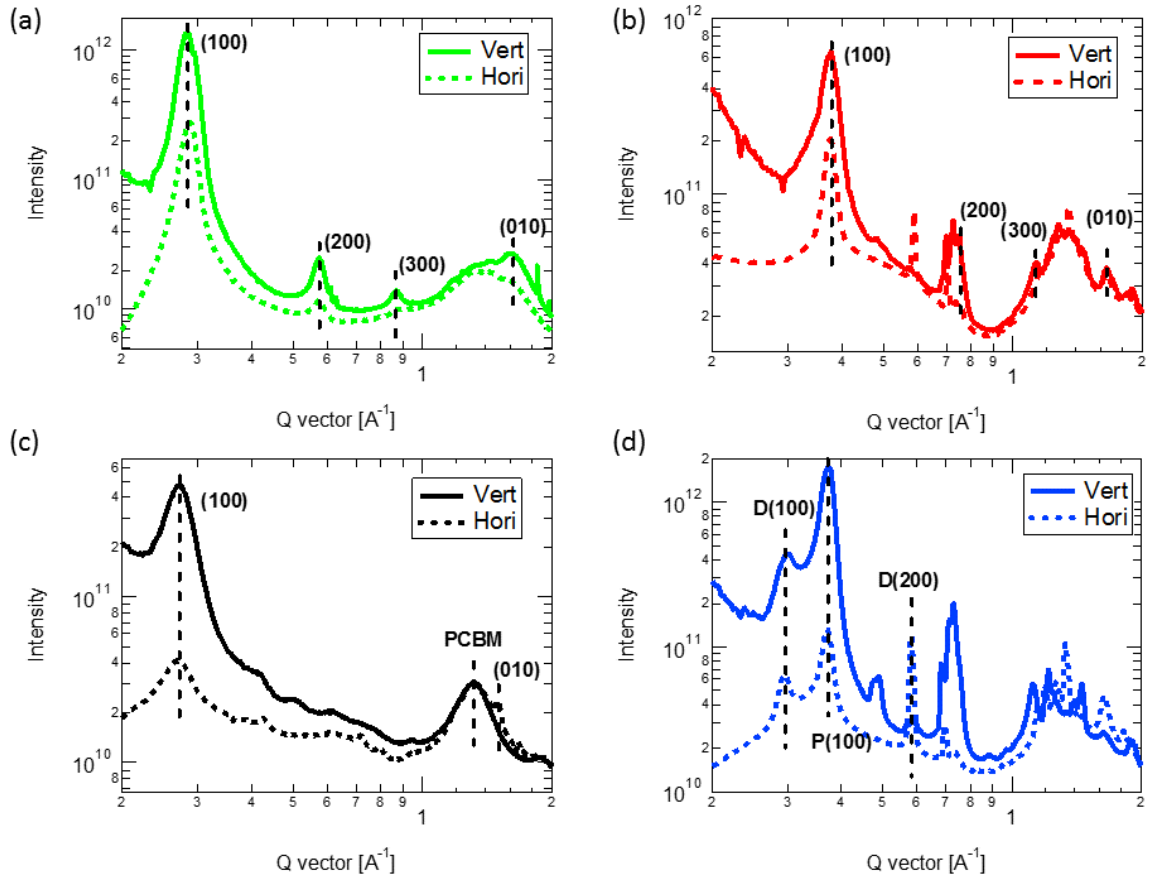

Figure S16. 1D GIWAXS profiles along out-of-plane (OOP, vertical) and in-plane (IP, horizontal) of pure 2DPP-BDT **(a)**, as-cast 2DPP-BDT:$PC_{71}BM$ **(b)**, thermally annealed P3HT:$PC_{71}BM$ **(c)** and P3HT:2DPP-BDT:$PC_{71}BM$ blend processed with 1-CN **(d)**. The subscript D denotes 2DPP-BDT and P denotes P3HT.

References:

(1) Shin, W.; Yasuda, T.; Hidaka, Y.; Watanabe, G.; Arai, R.; Nasu, K.; Yamaguchi, T.; Murakami, W.; Makita, K.; Adachi, C. π -Extended Narrow-Bandgap Diketopyrrolopyrrole-Based Oligomers for Solution-Processed Inverted Organic Solar Cells. *Adv. Energy Mater.* **2014**, *4*, 1400879.

(2) Kirby, N. M.; Mudie, S. T.; Hawley, A. M.; Cookson, D. J.; Mertens, H. D. T.; Cowieson, N.; Samardzic-Boban, V.; IUCr. A Low-Background-Intensity Focusing Small-Angle X-Ray Scattering Undulator Beamline. *J. Appl. Crystallogr.* **2013**, *46*, 1670–1680 .

(3) Ilavsky, J.; IUCr. *Nika* : Software for Two-Dimensional Data Reduction. *J. Appl. Crystallogr.* **2012**, *45*, 324–328.

(4) Lakowicz, J. R. *Principles of Fluorescence Spectroscopy*; 2006.